HE Emission from Magnetars

Zorawar Wadiasingh

Matthew G. Baring
Peter L. Gonthier
Alice K. Harding

Pulsar Magnetospheres Workshop @ Goddard June 6-8, 2016

Magnetars: Pulsars with B $\sim 10^{14}$ G — Not rotation-powered!

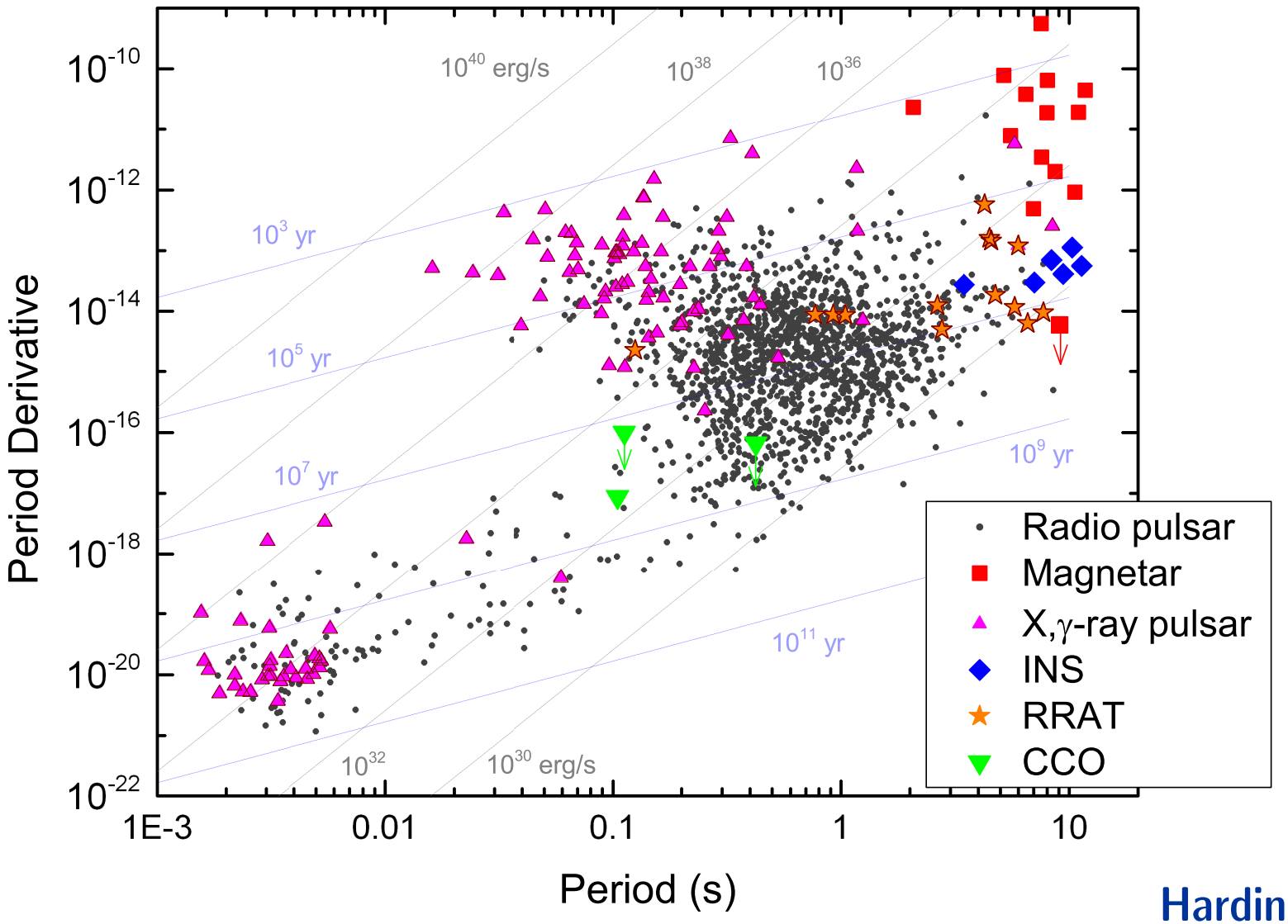

Harding 2013

INTEGRAL/RXTE Spectrum for AXP 1RXJS J1708-4009

- XMM spectrum below 10 keV dominates pulsed RXTE/PCA spectrum (black crosses);
- RXTE-PCA (blue) + RXTE-HEXTE (acqua) and INTEGRAL-ISGRI (red) spectrum in 20-150 keV band is not totally pulsed, with E^{-1}.
- COMPTEL upper limits imply spectral turnover around 300-500 keV, indicated by logparabolic guide curve.

Den Hartog et al. (2008)

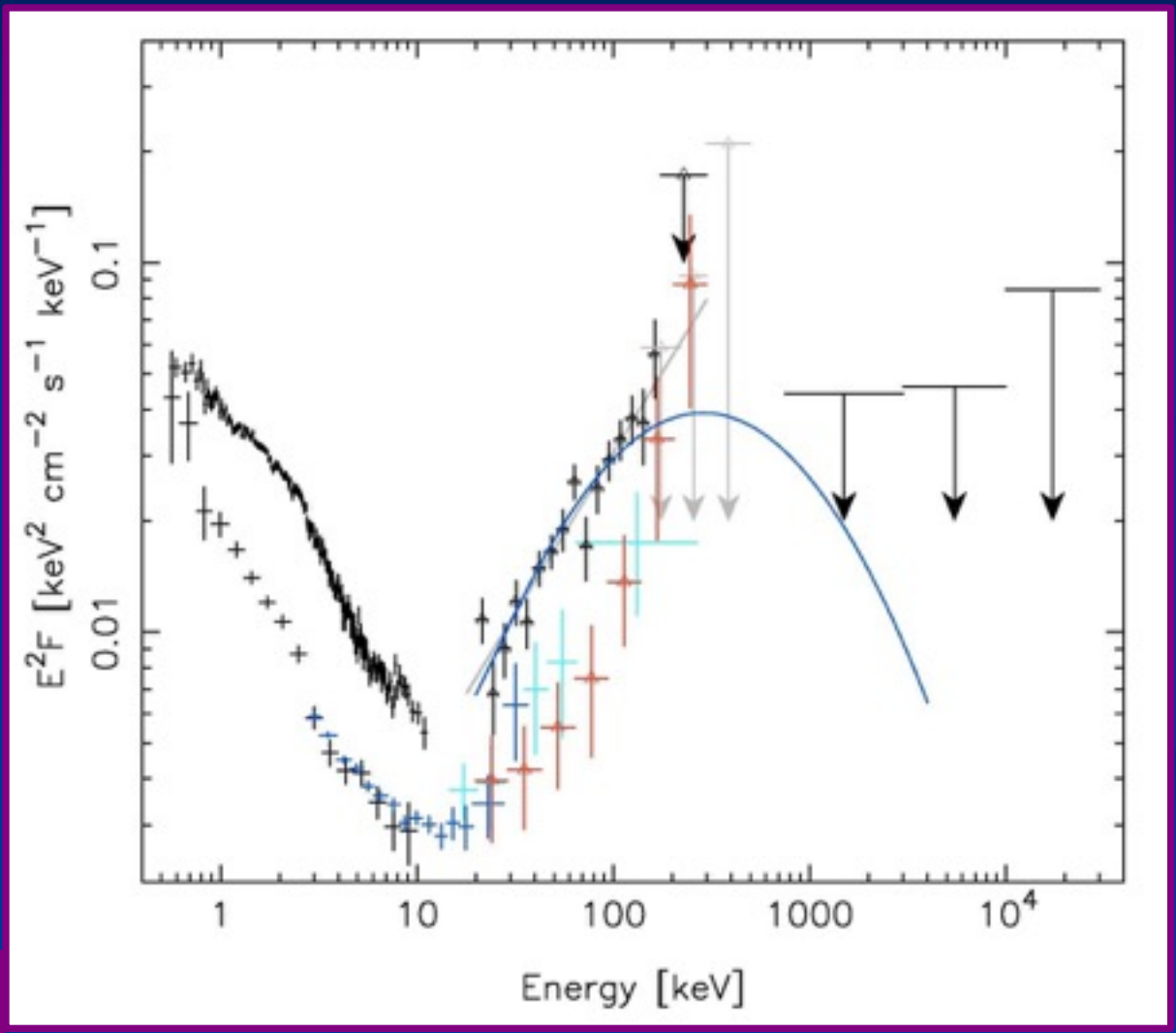

Magnetar Pulse Profiles in Soft and Hard Bands

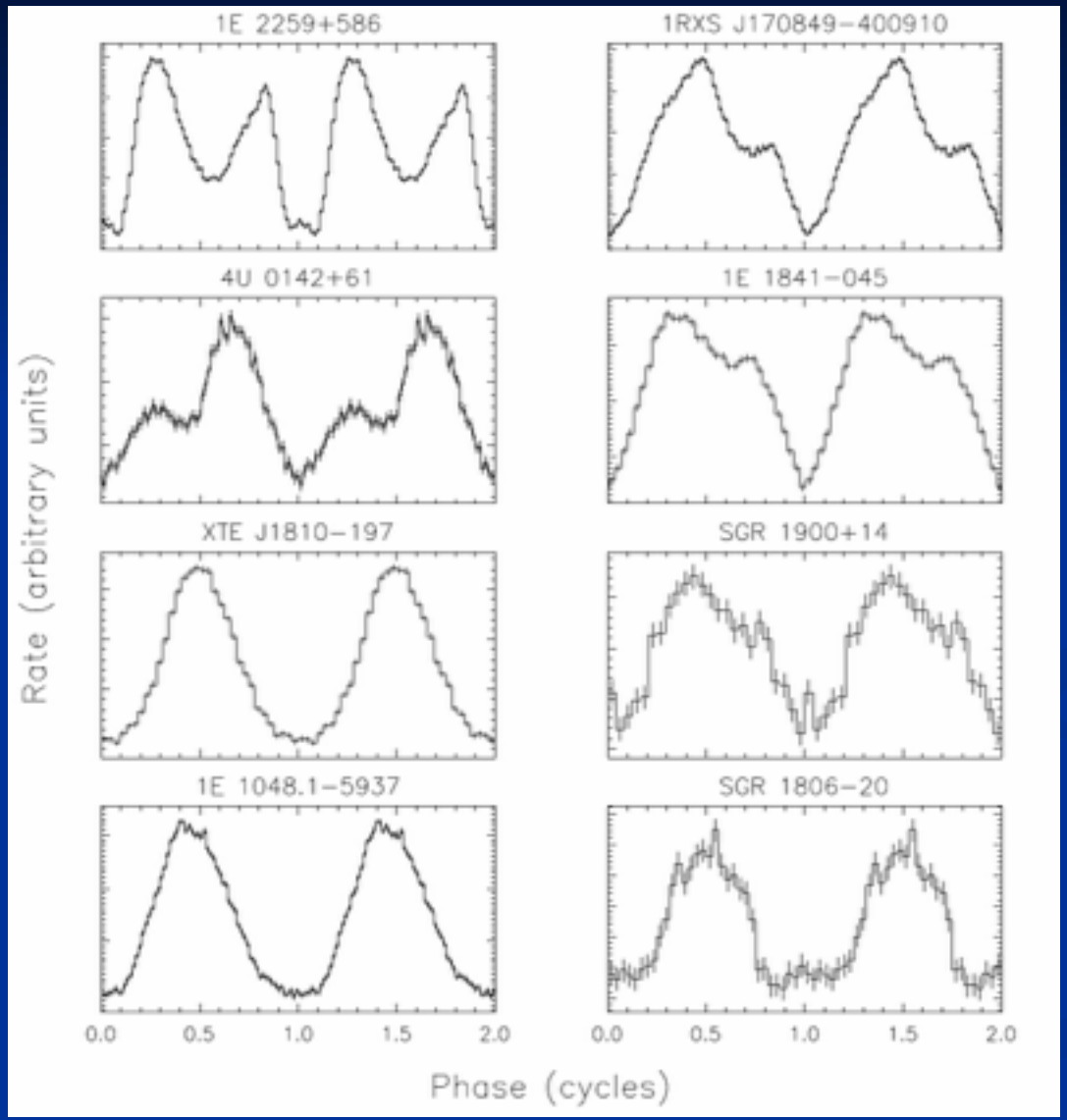

Woods & Thompson 2006

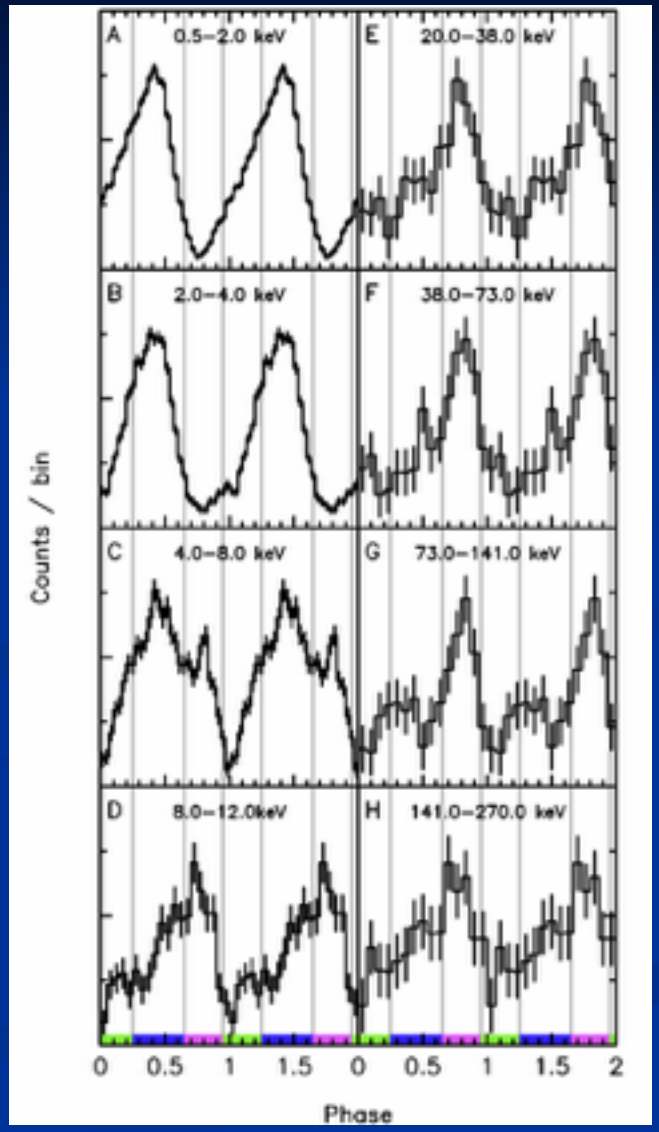

den Hartog et al. 2008

Resonant Compton Cross Section (ERF)

- Illustrated for photon propagation along B and the Johnson & Lipmann formalism;
- In magnetar fields, cross section declines due to Klein-Nishina reductions;
- Resonance at cyclotron frequency $eB/m_e c$;
- Below resonance, *l=0* provides contribution;
- In resonance, cyclotron decay width truncates divergence.

B = 1 => B = 4.41 x 10^{13} G

Gonthier et al. 2000

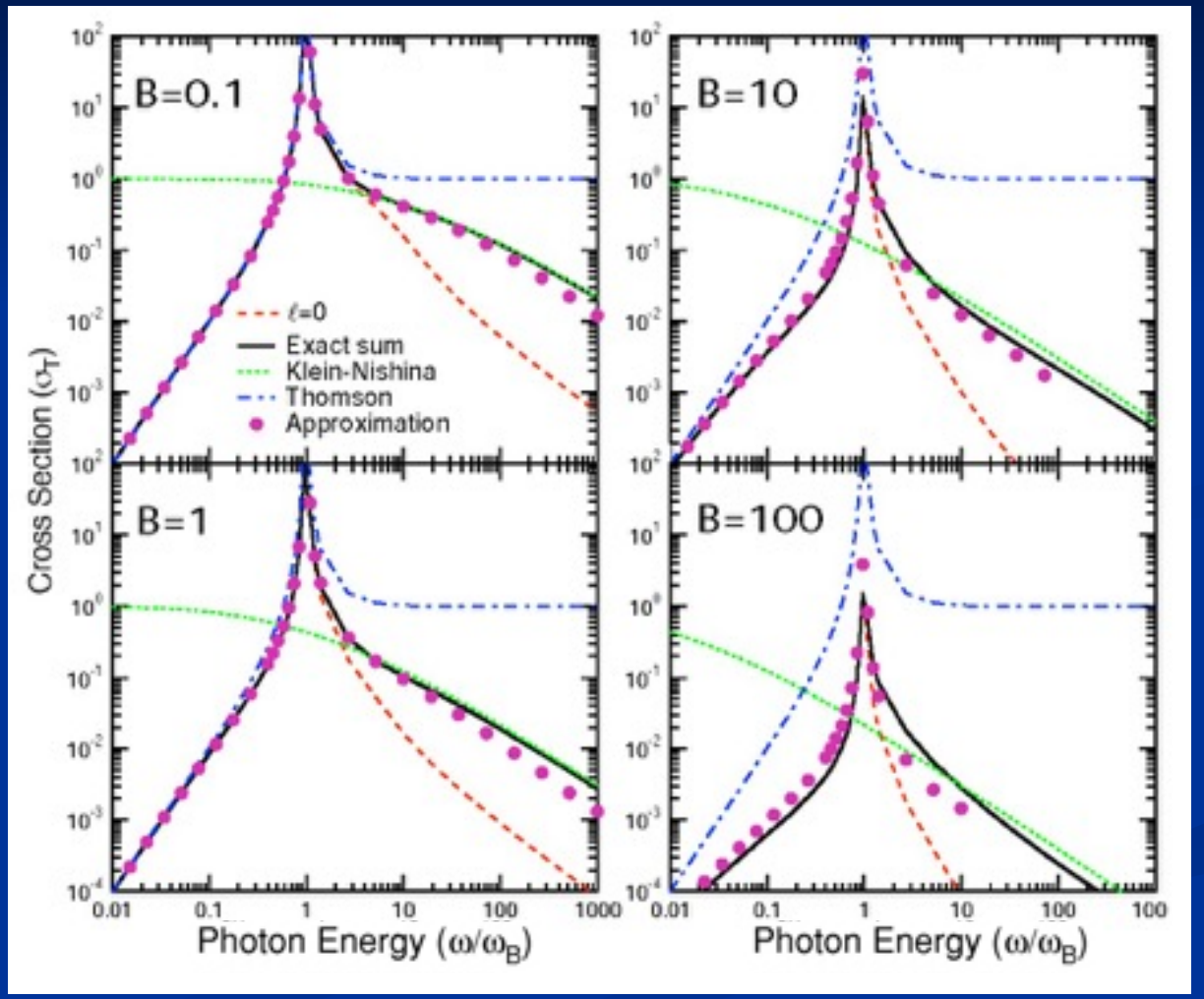

Polarization Dependence of Resonant Compton Cross Section

Gonthier et al. 2000

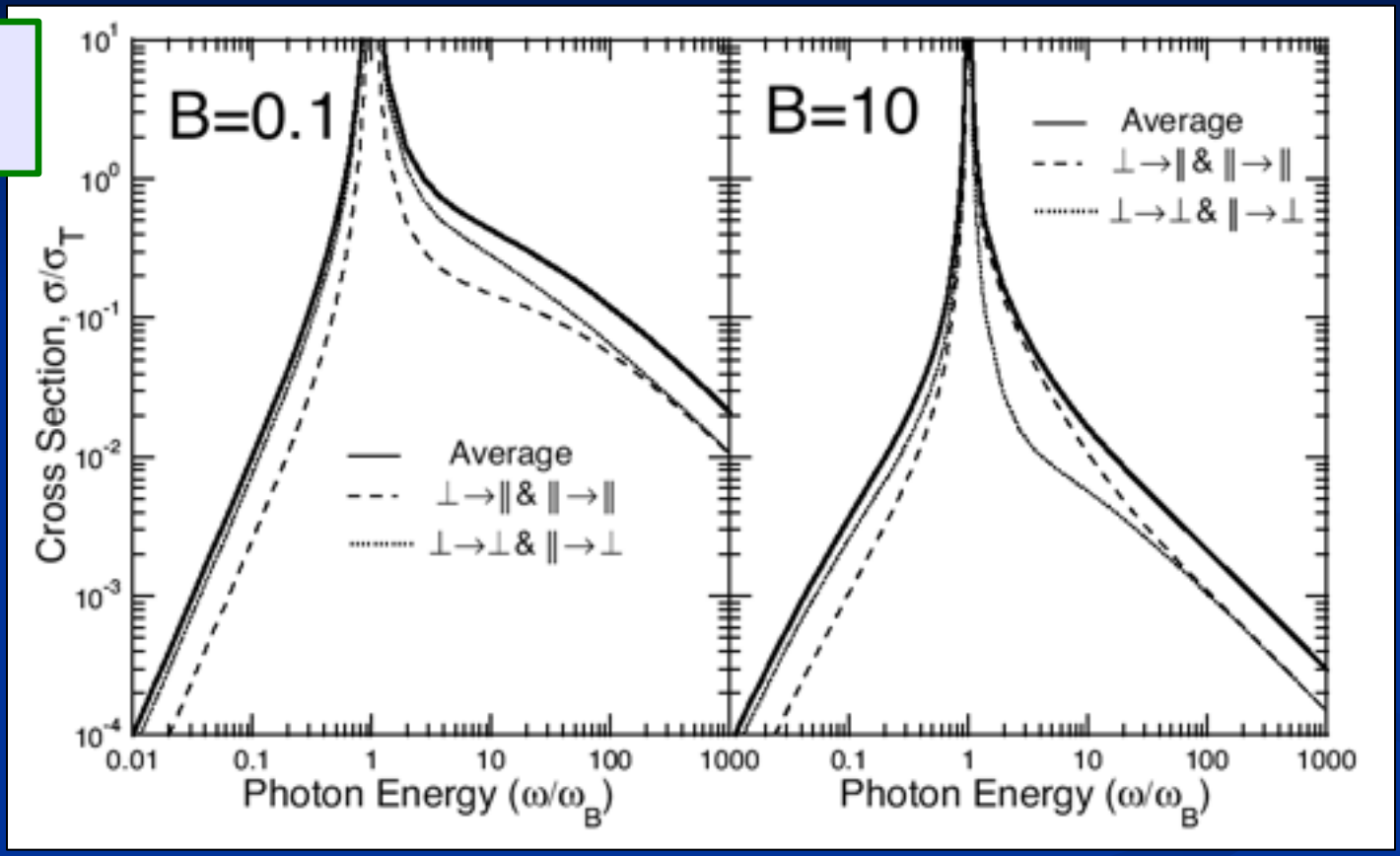

- Differential and total cross section depend only on final polarization state of photons;
- Perpendicular polarization "extraordinary mode" (E-field ⊥ to plane spanned by k & B) exceeds parallel ;
- Cooling calculations sum/average over polarization states.

ST Cyclotron Decay Lifetimes for the Resonance

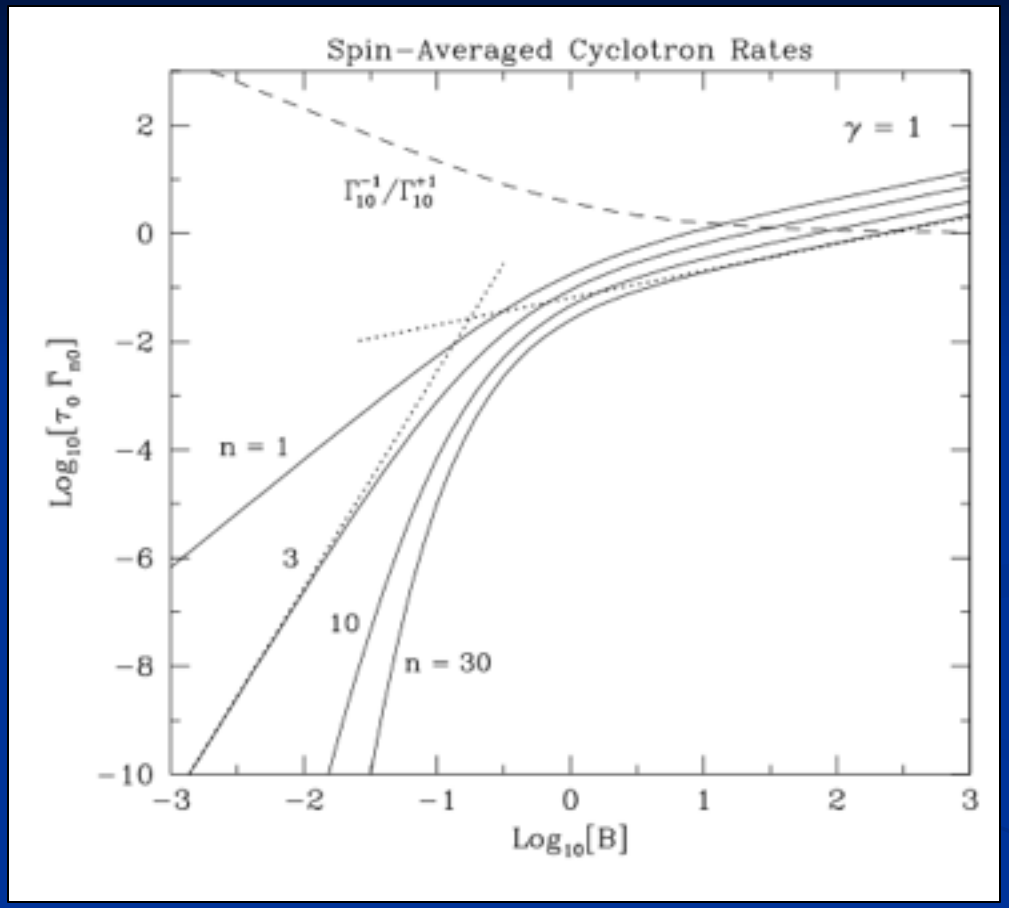

Baring, Gonthier & Harding (2005)

- Cyclotron decay B^2 field dependence is muted to $B^{1/2}$ dependence in supercritical fields (e.g. Herold et al. 1982; Latal 1986; Pavlov et al. 1991). These rates set the "cap" on the Compton resonance via a width in a Lorentz profile.

Spin-dependent rates – the problem with Johnson & Lippmann states

Sokolov & Ternov states (1968) preserve separability of the spin dependence under Lorentz boosts along B.

However, Johnson & Lipmann states (1949) do not!

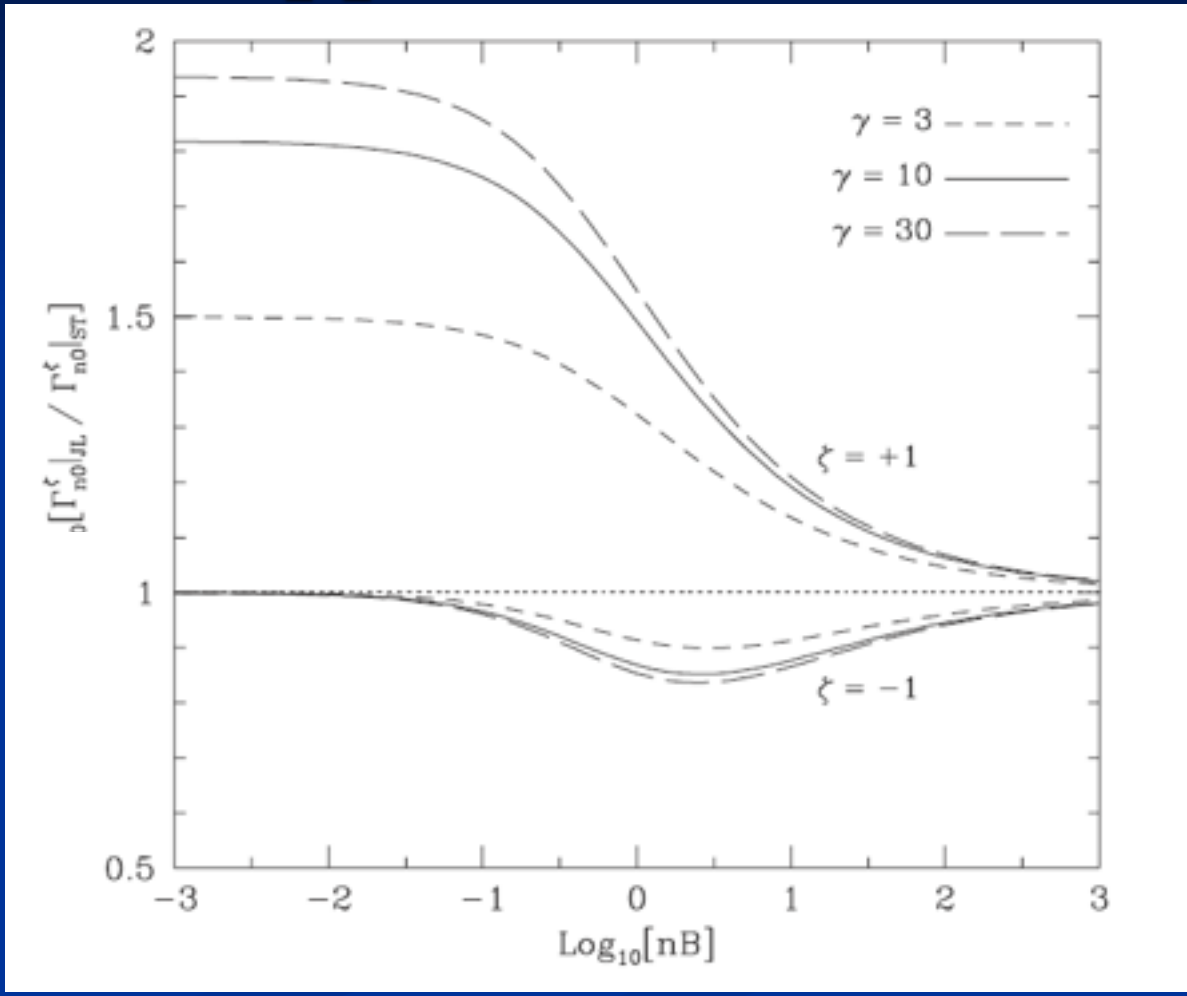

Baring, Gonthier & Harding 2005

JL versus ST states

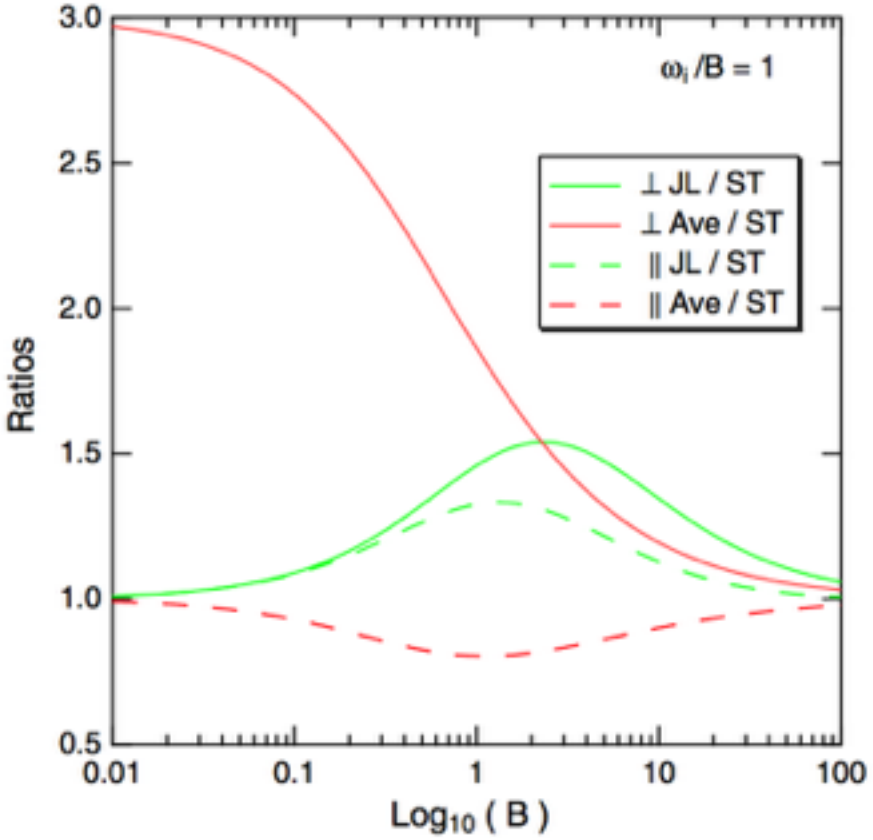

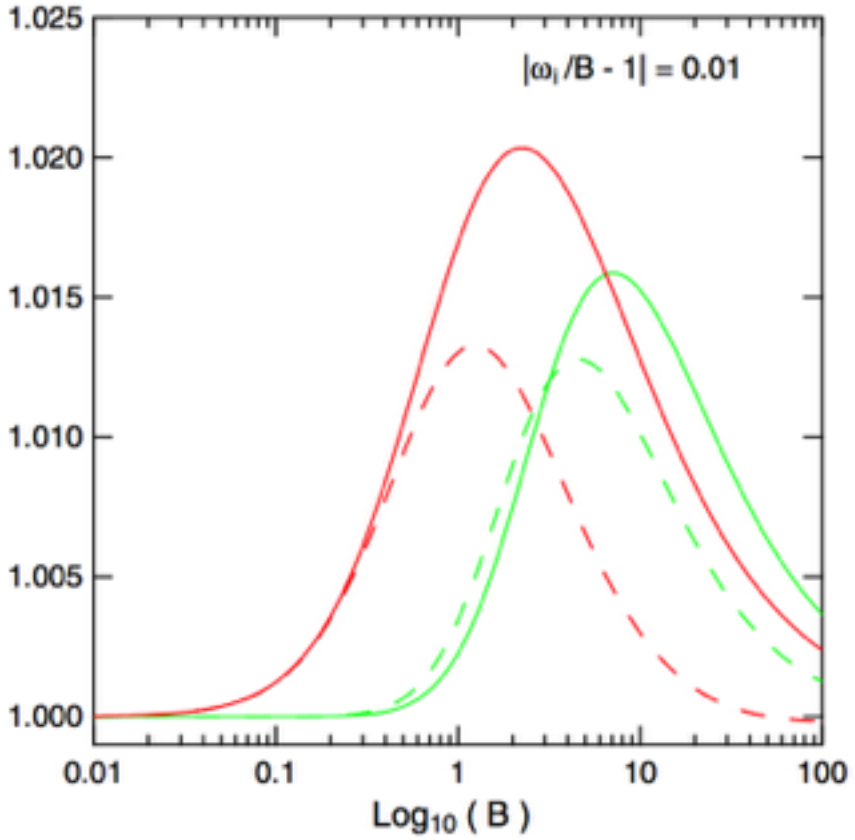

Compton Upscattering Kinematics

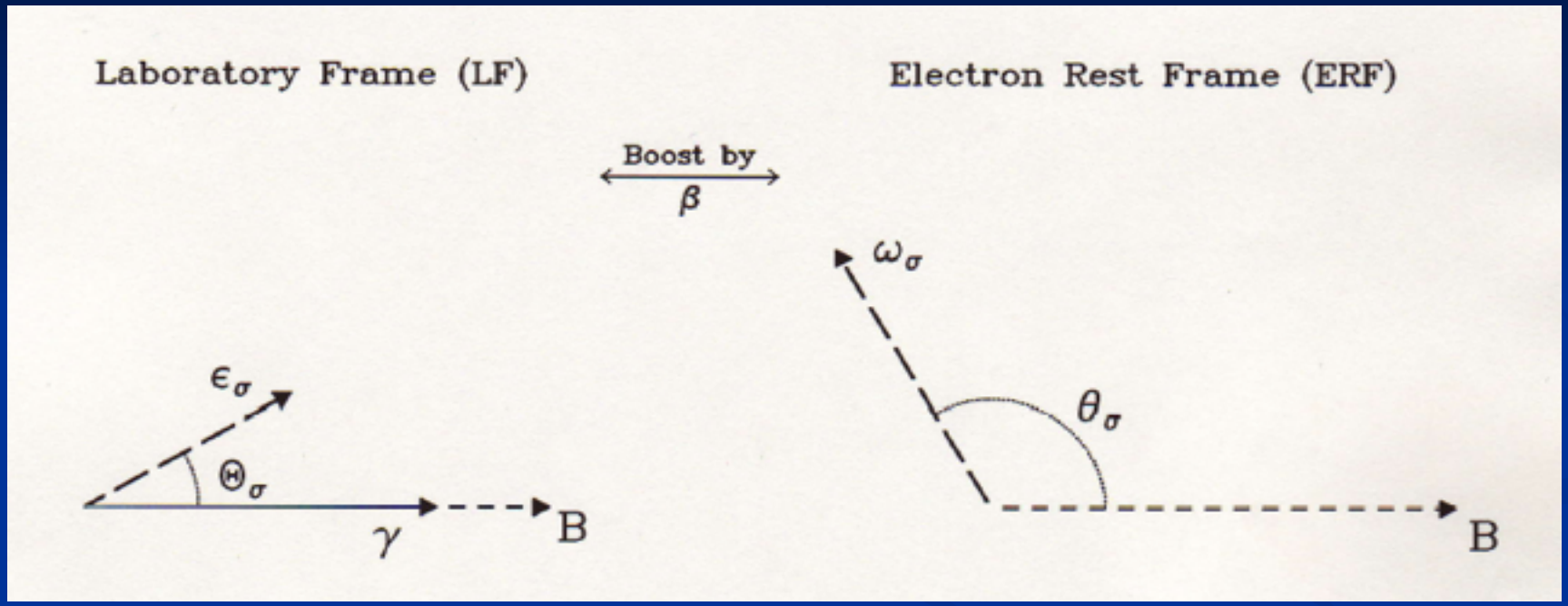

- Upscattering kinematics is often controlled by the criterion for scattering in the cyclotron resonance: there is a one-to-one correspondence between final photon angle to B and upscattered energy.

$$\gamma\varepsilon_i(1-\beta\cos\theta_{kB,i}) \approx B \sim \gamma\varepsilon_f(1-\beta\cos\theta_{kB,f})$$

Resonant Compton Kinematics

• Resonant Compton interactions in magnetars and high **B** pulsars predominantly correspond to *ground state-to-ground state* $i \to f$ *transitions*: Landau level quantum numbers are zero.

• Kinematics in the electron rest frame (ERF) in this special case are described by (for $\theta_i = 0$)

$$\omega_f = \frac{2\omega_i}{1 + \omega_i(1 - \cos\theta_f) + \left[(1 + \omega_i(1 - \cos\theta_f))^2 - 2\omega_i \sin^2\theta_f\right]^{1/2}} ,$$

where $\omega_i \equiv \omega$, ω_f are photon energies scaled by $m_e c^2$.

• This includes Klein-Nishina regime recoil contributions, and when $\omega \ll 1$, this formula reduces to the familiar Compton one for $B = 0$ scattering.

High B Resonant Compton Cooling

Baring, Wadiasingh & Gonthier 2011

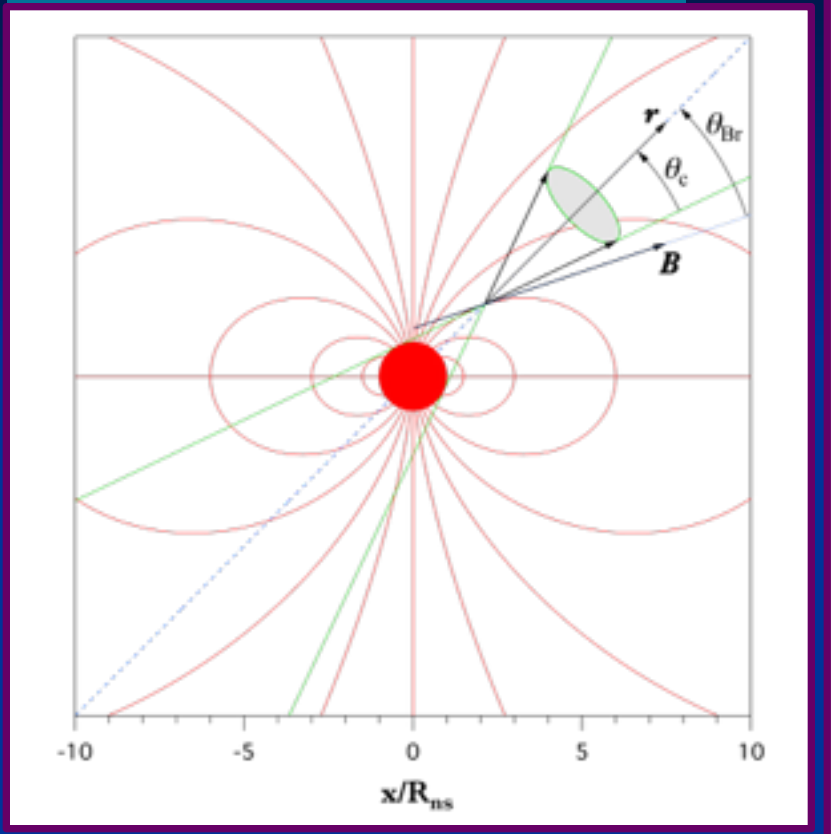

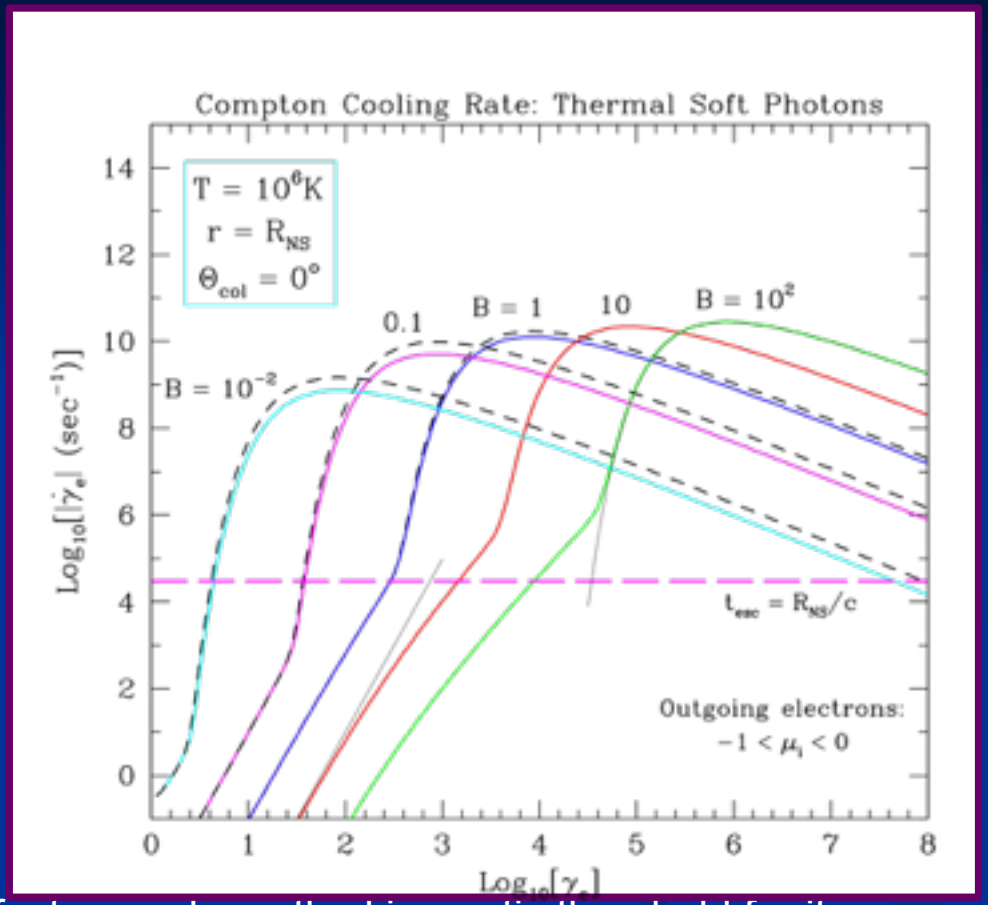

- Resonant cooling is strong for all Lorentz factors γ above the kinematic threshold for its accessibility; magnetic field dependence as a function of B is displayed at the right (dashed lines denote JL spin-averaged calculations, instead of the spin-dependent ST cross section).
- Kinematics dictate the B dependence of the cooling rate at the Planckian maximum. For magnetar magnetospheres, Lorentz factors following injection are limited to ~10^1-10^3 by cooling.

Thermal Cooling Rates

- Monoenergetic cooling rates integrated over a Planck spectrum;
- Resonance is always sampled, and there is a strong dependence on T;
- Ingoing versus outgoing electrons alter where the resonance is sampled.

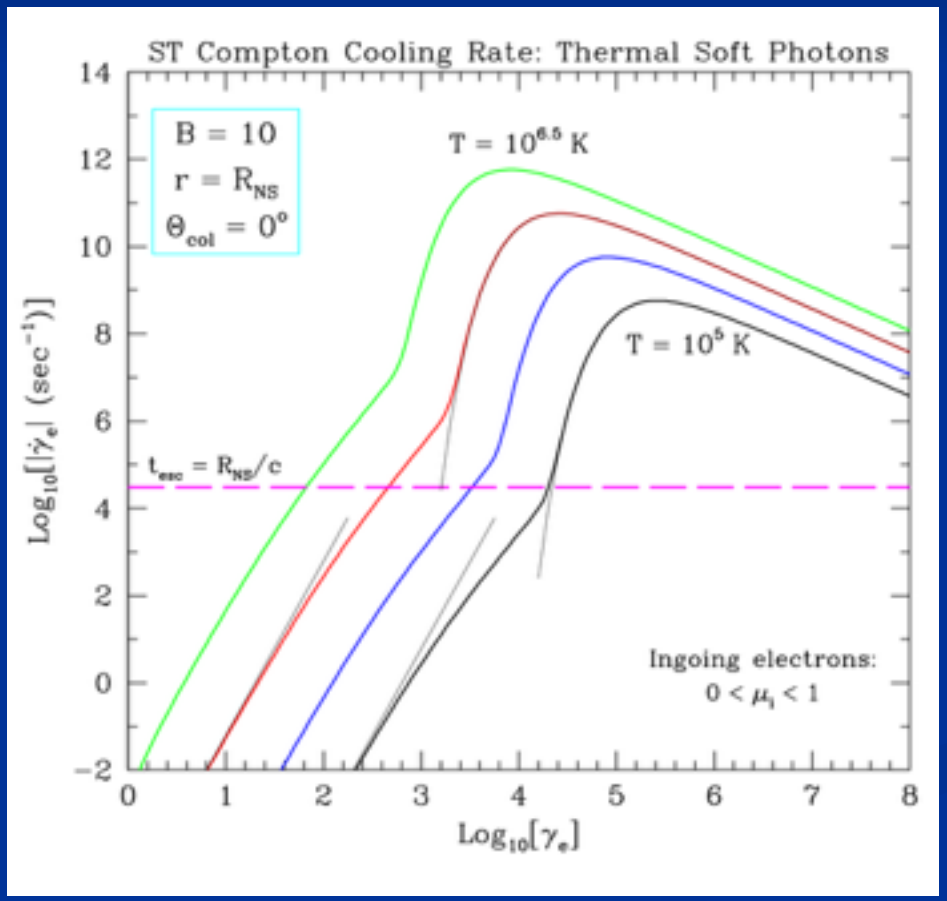

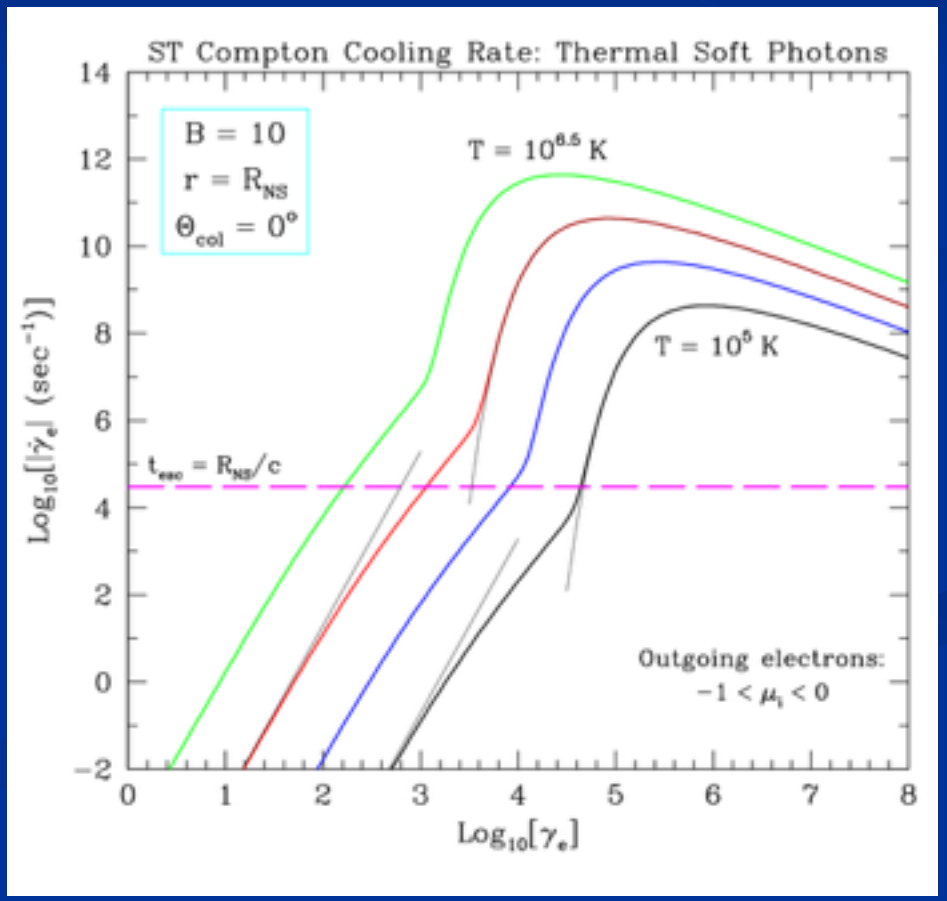

Altitudinal Dependence

- The photon angular distribution changes the altitudinal character of the cooling rate at various co-latitudes;
- Shown here are the two extreme cases;
- The outgoing electrons case at the equator is equivalent to the ingoing electrons case due to the symmetry of the photon distribution.

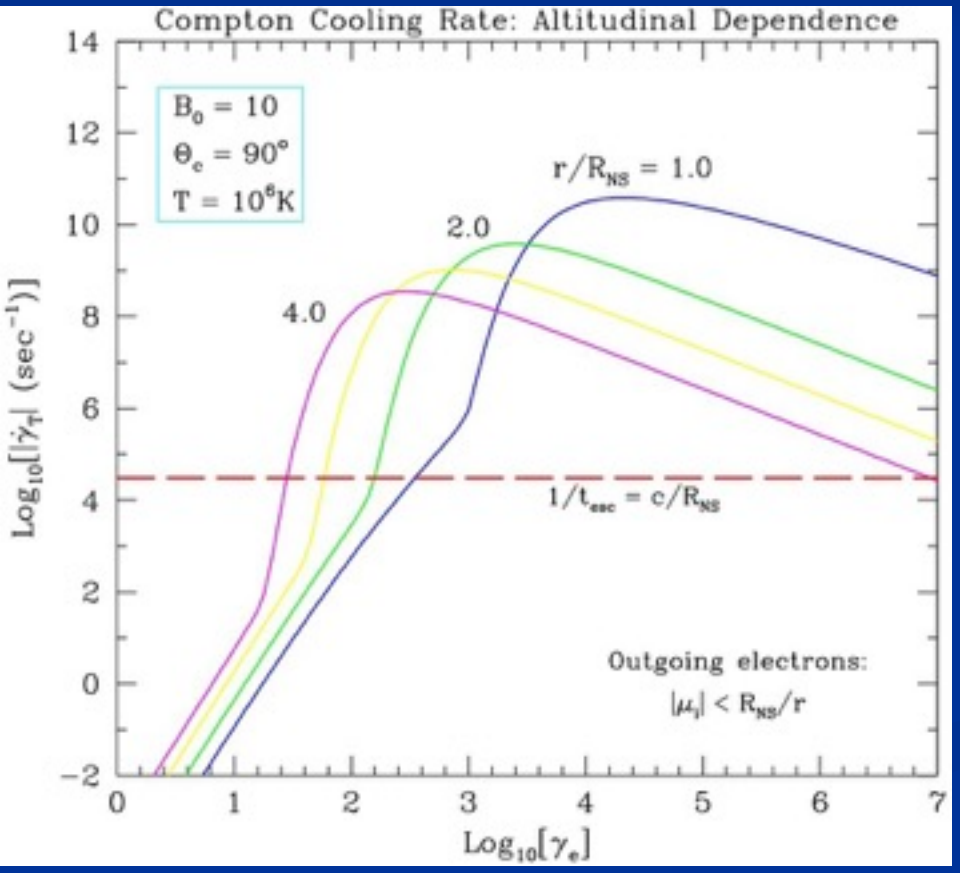

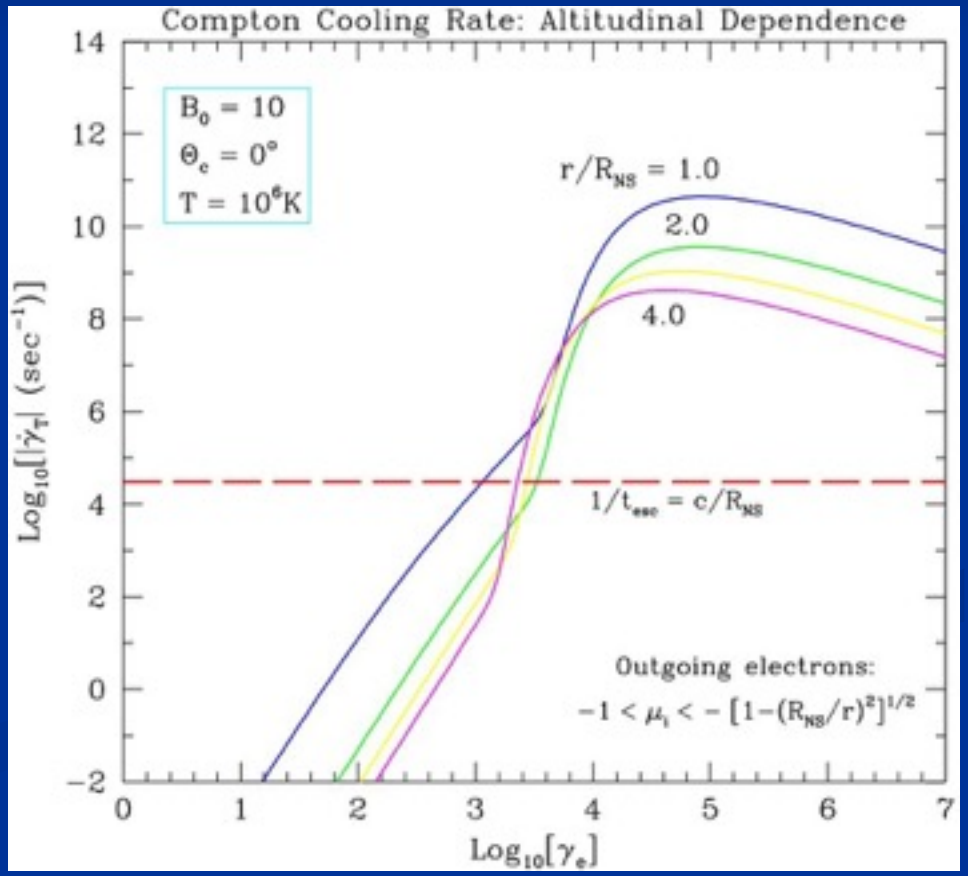

Resonant Scattering: Orthogonal Projections

- Black points bound the locii ("green" and "blue") of final scattered energies of greater than $\varepsilon_f = 10^{-0.5}$ => 160 keV;
- For most viewing angles, this is a very small portion of the activated magnetosphere for the Lorentz factor and polar field chosen below.

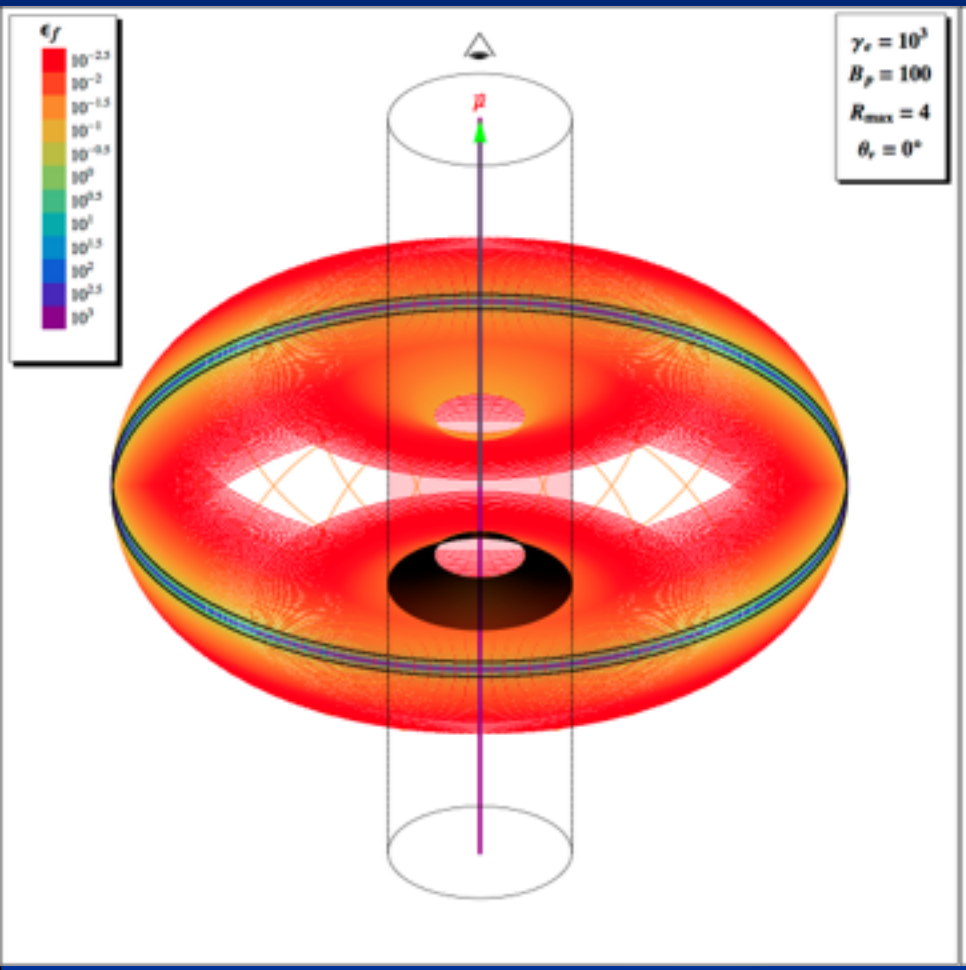

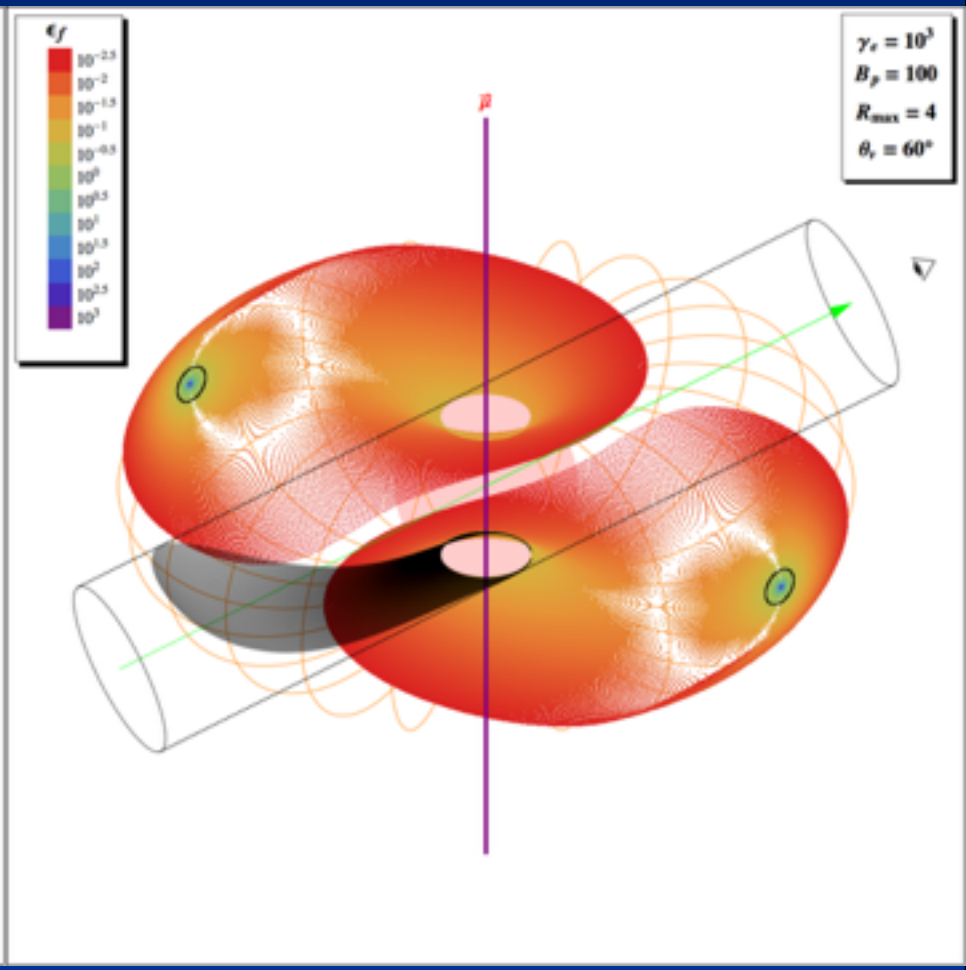

Observer Perspectives and Resonant Scattering Kinematics

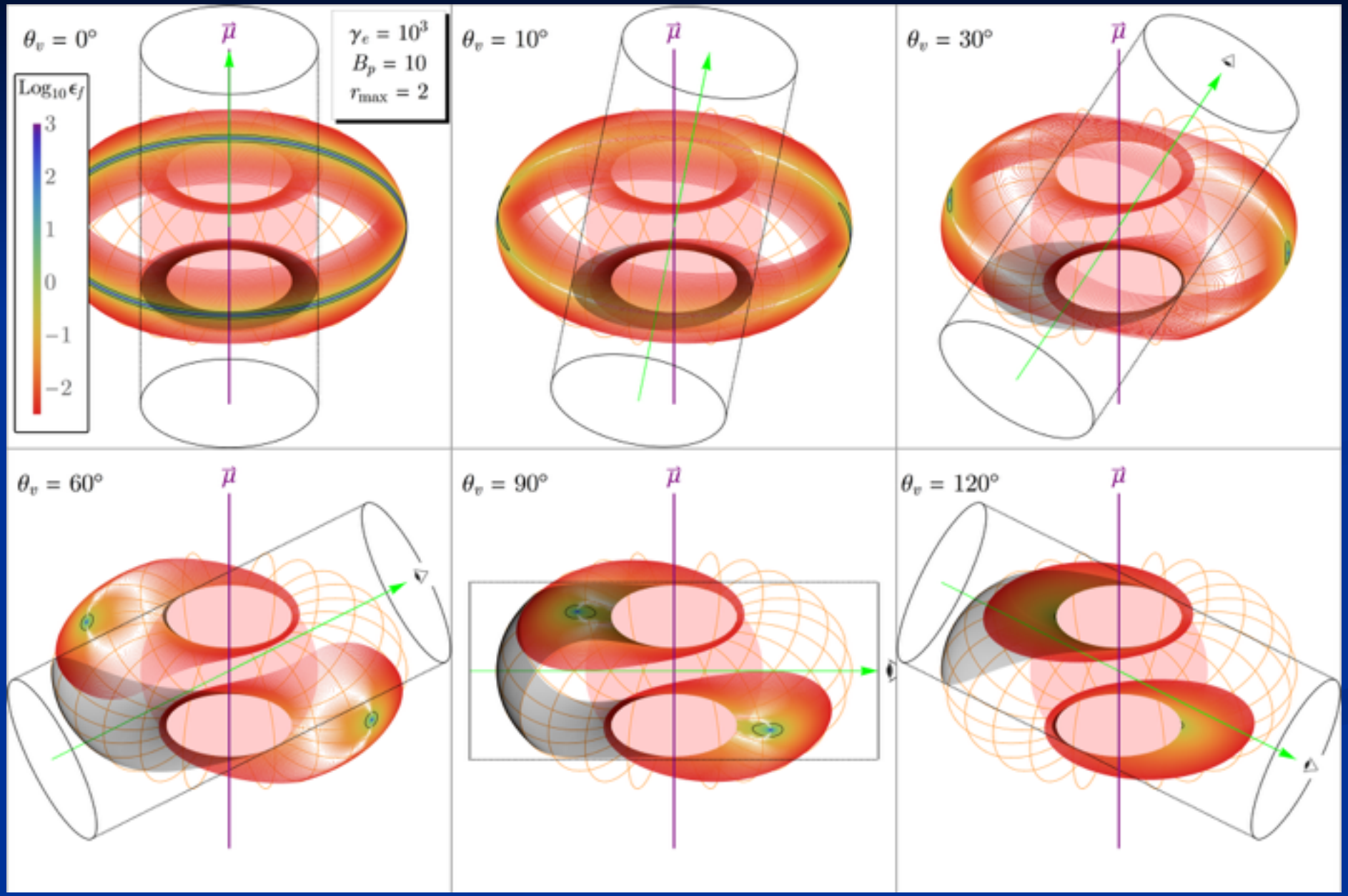

Template(single field loop) Polarization-dependent Spectra

Strong polarization at high energies

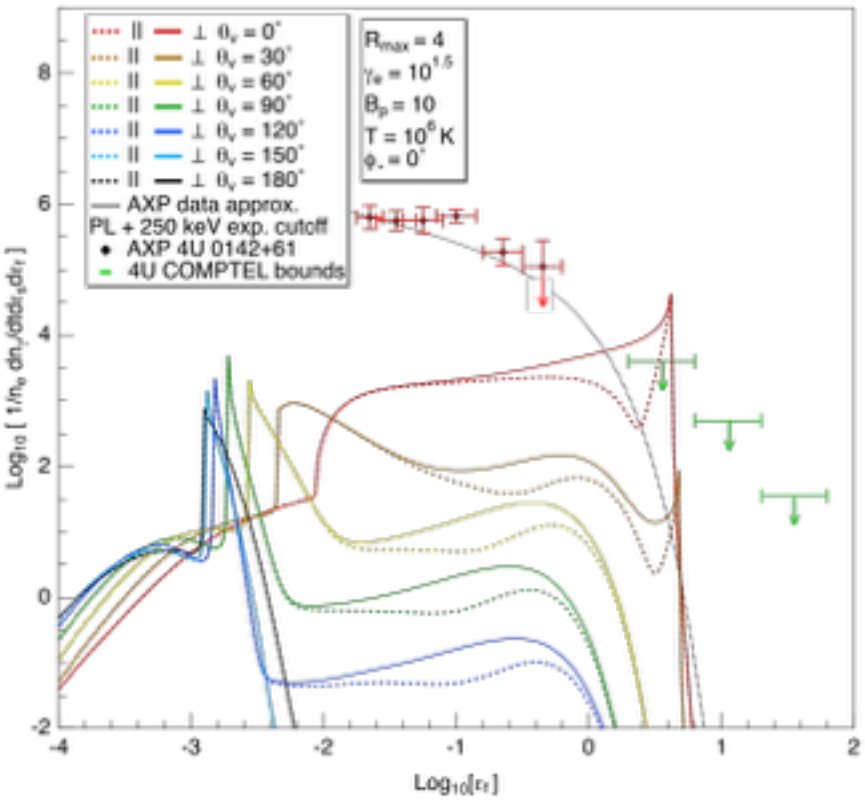

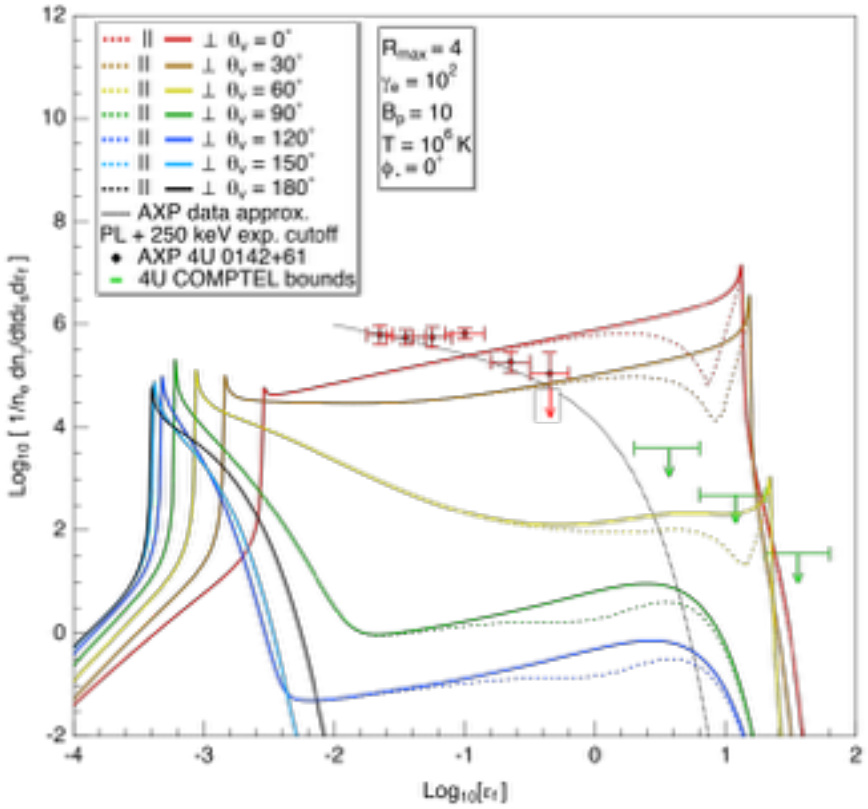

Maximum Energy w.r.t. Rotation Phase

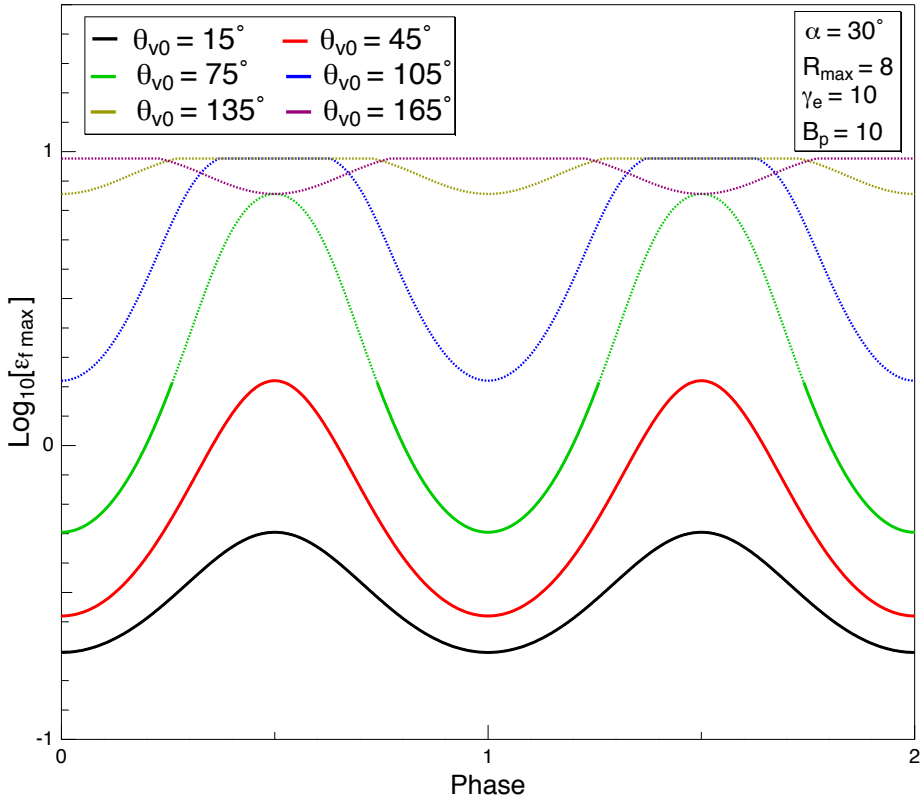

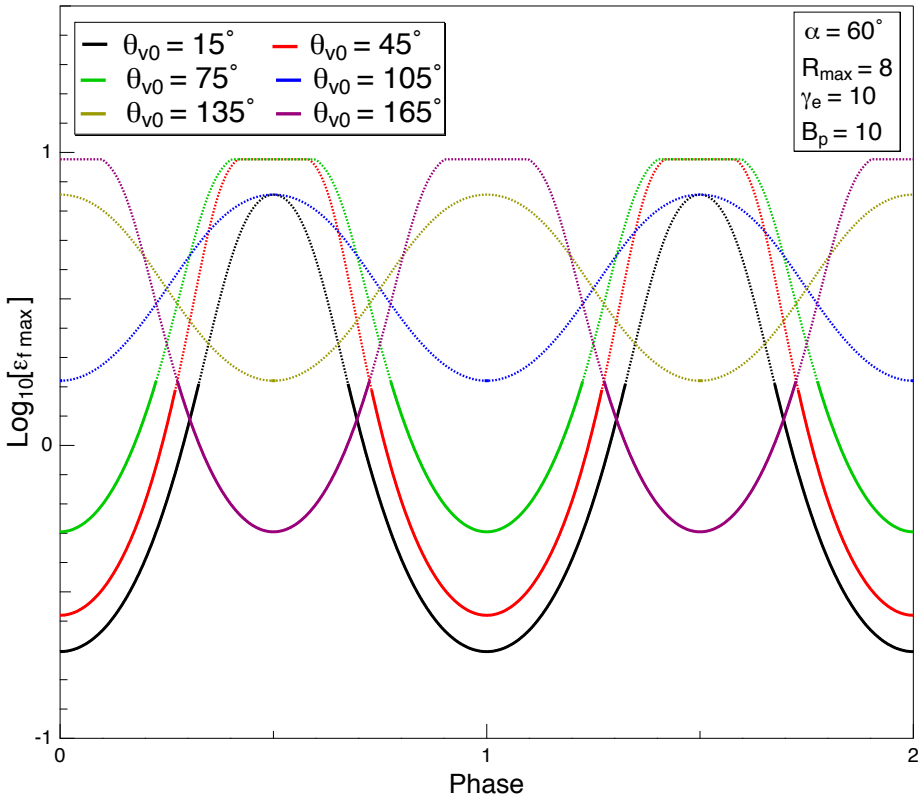

Radiative Transport $\gamma B \rightarrow e^+e^-$

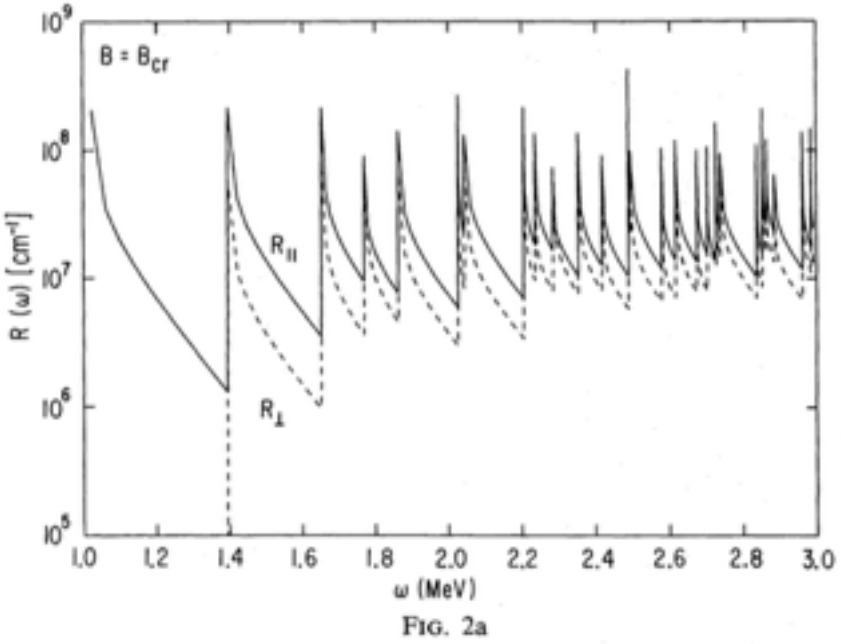

FIG. 2a

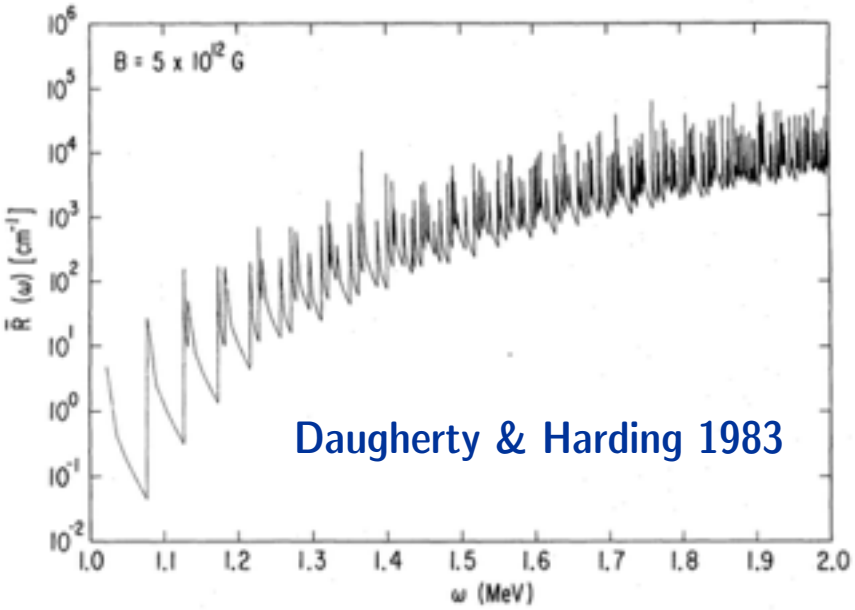

Daugherty & Harding 1983

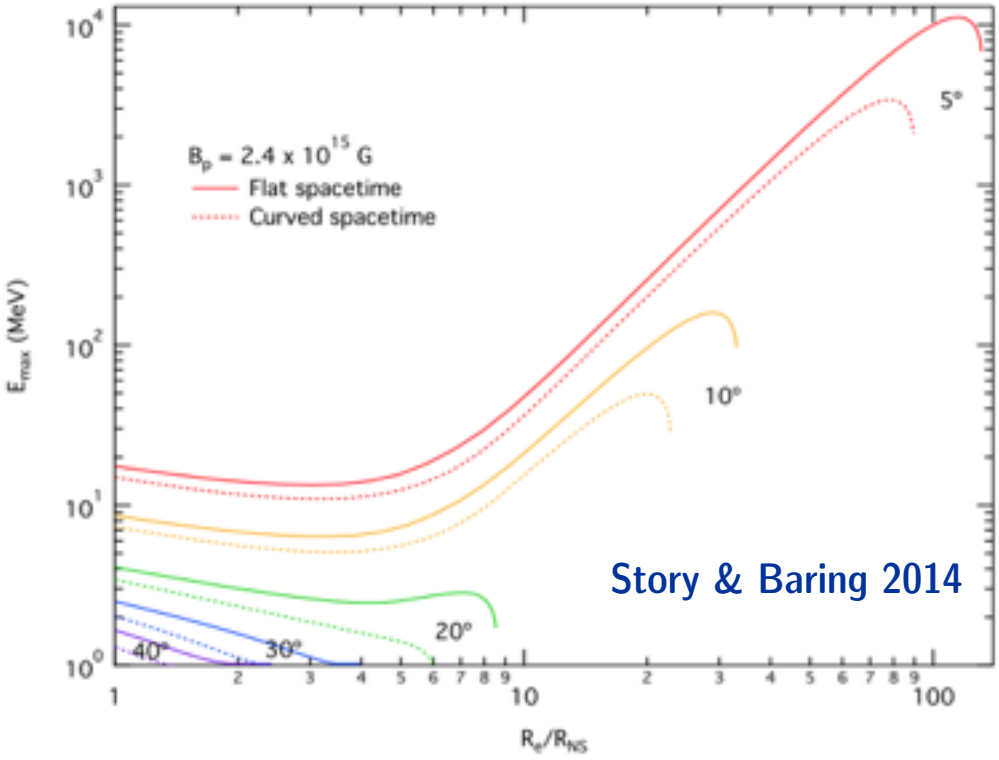

Story & Baring 2014

- Pair creation escape energies limits >1 MeV photons in magnetars based on emission height

Radiative Transport, Magnetic Photon Splitting $\gamma B \rightarrow \gamma\gamma$

- Resonant ICS — $\perp$ dominates $\parallel$ at higher energies
- Magnetic pair creation, only above the 2 $m_e c^2$ threshold — R $\parallel$ > R $\perp$
- $\perp \rightarrow \parallel \parallel$ is the only allowed mode from kinematic selection rules (Adler 1971) when vacuum dispersion is small ==> weak splitting cascade
- CP symmetry of QED allows: $\perp \rightarrow \parallel \parallel$, $\perp \rightarrow \perp \perp$, $\parallel \rightarrow \perp \parallel$ ==> splitting cascade can be a strong attenuation influence

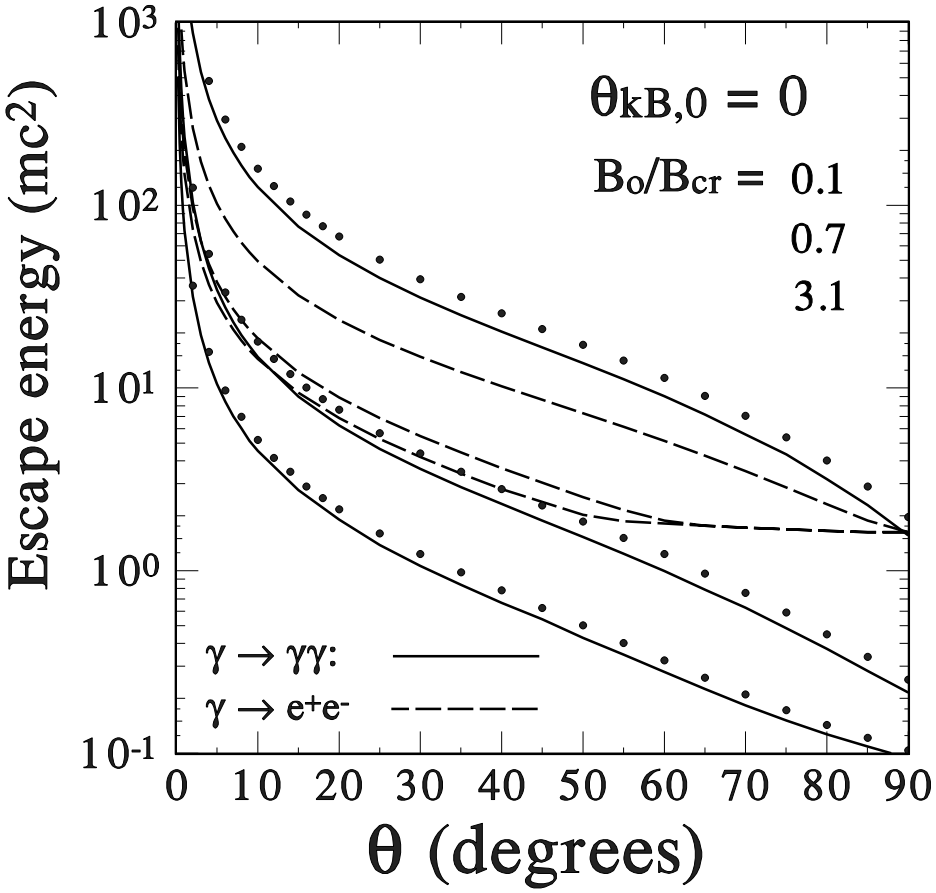

Harding, Baring & Gonthier 1997

3rd order

$$T_{sp}(\omega) \approx \frac{\alpha^3}{10\pi^2}\frac{1}{\lambda}\left(\frac{19}{315}\right)^2 B'^6 \mathscr{C}(B')\omega^5 \sin^6\theta_{kB}$$

Vacuum Birefringence => Crystal "optical axis" <—> local B direction

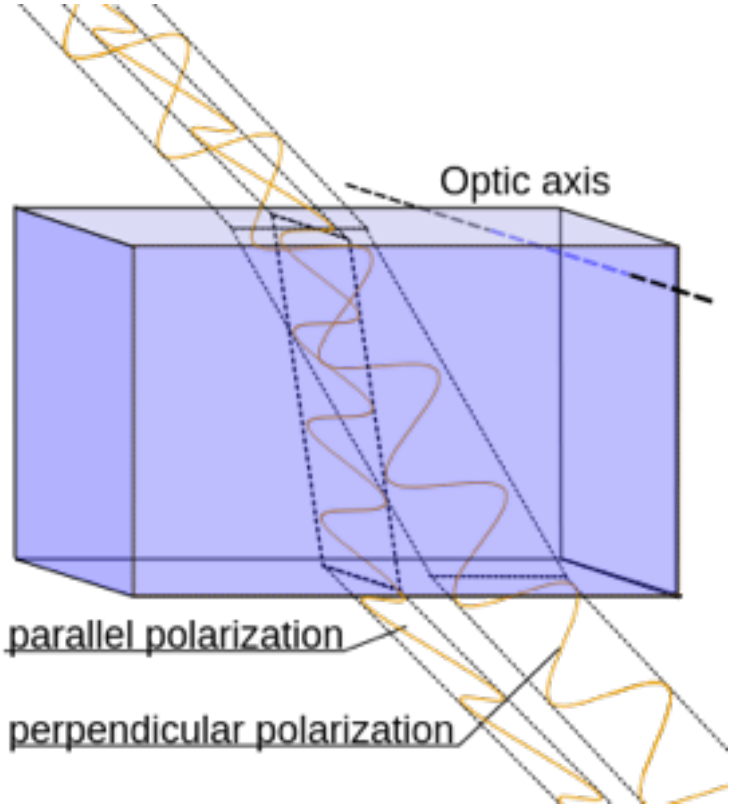

- Virtual magnetic pair creation (dominant contribution) and other QED diagrams make the vacuum birefringent perpendicular to B
- Polarizations can get mixed/ rotated as they propagate out, depending on the path!
- Vacuum: $n_{||} > n_{\perp}$ typically for most magnetar regimes
- Plasma effects also mix states
- **Need a soft γ-ray polarimeter with good energy and time resolution to disentangle emission geometry, reaching down to ~50-100 keV**

$$n_{\perp} \approx 1 + \frac{\alpha_f}{6\pi}\sin^2\theta, \qquad n_{\perp} \approx 1 + \frac{2\alpha_f}{45\pi}B^2\sin^2\theta,$$

$$n_{\parallel} \approx 1 + \frac{\alpha_f}{6\pi}B\sin^2\theta, \quad B \gg 1 \qquad n_{\parallel} \approx 1 + \frac{7\alpha_f}{90\pi}B^2\sin^2\theta, \quad B \ll 1$$